J. Fluid Mech. (1972), *vol.* 53, *part* 2, *pp.* 329–349
Printed in Great Britain

Two-dimensional sink flow of a stratified fluid contained in a duct

By JORG IMBERGER

Departments of Mathematics and Hydraulics, University of California, Berkeley†

(Received 26 August 1971)

A reservoir is assumed to be filled with water which has a linear variation of density with depth. The geometry of the boundaries is simplified to a parallel walled duct with the line sink at the centre of the fluid. The primary focus is on partitioning the flow into distinct flow regimes and predicting the withdrawal-layer thickness as a function of the distance from the sink; the predictions are verified experimentally.

For fluids with a Schmidt number of order unity, the withdrawal layer is shown to be composed of distinct regions in each of which a definite force balance prevails. The outer flow, where inertia forces are neglected, changes from a parallel uniform flow upstream to a symmetric self-similar withdrawal layer near the sink. For distances from the sink smaller than a critical distance, dependent on the flow parameters, inertia forces become of equal importance to buoyancy and viscous forces. The equations valid in this inner region are derived. Using the inner limit of the outer flow as the upstream boundary condition, these inner equations are solved approximately for the withdrawal-layer thickness by an integral method. The inner and outer variations of δ, the withdrawal-layer thickness, are combined to yield a composite solution and it is seen that the inclusion of inertia forces yields layers thicker than those obtained from a strict buoyancy–viscous force balance. In terms of the inner variables the only parameter remaining is the Schmidt number.

Laboratory experiments were carried out to verify the theoretical conclusions. The observed withdrawal-layer thicknesses were shown to be closely predicted by the integral solution. Furthermore, the data could be represented in terms of the inner variables by a single curve dependent only on the Schmidt number.

1. Introduction

In spring and summer the impounded water of a storage reservoir usually becomes stratified. A simplification often made in heat budget models of such reservoirs is to assume that this density gradient prohibits all vertical motion, and that water withdrawn comes from a very thin horizontal layer at the intake level. The purpose of this paper is to investigate both the detailed structure and the thickness of a withdrawal-layer originating from a line sink. Such layers have

† Present address: W. M. Keck Laboratory of Hydraulics and Water Resources, California Institute of Technology, Pasadena.

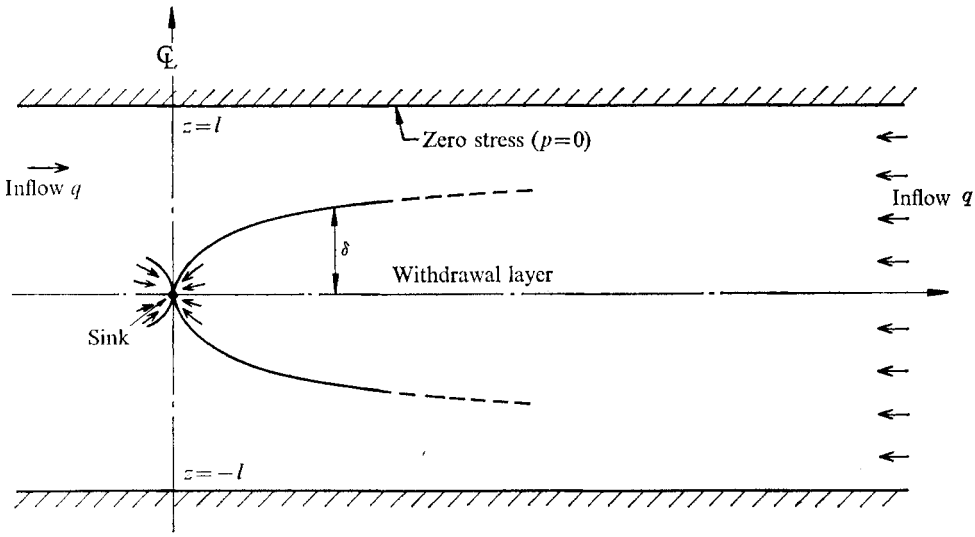

FIGURE 1. Theoretical model.

been investigated before, but with restrictive assumptions. It is instructive to recapitulate these solutions to see why they are unsatisfactory models of the withdrawal-layer phenomena in a large reservoir.

Yih (1965) assumed that the viscosity and the diffusivity of the fluid were zero. This leads to the Euler equations for a stratified fluid which, if one makes the assumption that upstream the density varies linearly with depth and that the product of the density and the velocity head is a constant, reduces to the Helmholtz equation for the stream function. For the boundary geometry shown in figure 1 this equation may be solved by standard methods and the solution is dependent on the magnitude of Froude number $F = U'_\infty/(g\epsilon d^2)^{\frac{1}{2}}$. U'_∞ is the modified upstream velocity and is equal to $(\rho/\rho_0)^{\frac{1}{2}}U_\infty$, where ρ is the density, ρ_0 the mean density and U_∞ the upstream velocity. The term $(g\epsilon)^{\frac{1}{2}}$ is the Brunt–Väisälä frequency. For $F > 1/\pi$ the solution is characterized by a nearly uniform flow towards the sink and an eddy in the upper corner. As the Froude number is decreased this eddy elongates, extending further upstream until at $F = 1/\pi$ the eddy streamlines close at infinity. Such flows violate the assumed upstream boundary condition, but the solution does indicate that a withdrawal layer forms as the Froude number is decreased.

In order to circumvent the difficulties associated with the eddy extending to infinity ($F < 1/\pi$), Kao (1965, 1970) introduced a slip line within the flow field, thus separating the flowing fluid from a stagnant upper layer. The results of Kao's work, especially the later paper, suggest that the Froude number, based on the flowing depth, remains constant and equal to $1/\pi$ independently of the discharge q and that the thickness of the layer is of the order of $F^{\frac{1}{2}}$.

However, there remains the question of what role viscosity plays in such a layer. Kao (1970) showed that the velocity of the fluid moving along the inside of the slip line was constant and of order $q^{\frac{1}{2}}(\epsilon g)^{\frac{1}{4}}$, where q is the sink discharge. This means that viscosity will cause a thin sublayer to grow around the upper

and lower slip lines in the upstream direction. Hence, at some point upstream the two sublayers will meet and viscosity will be important throughout the whole depth of the original withdrawal layer. The natural upstream boundary condition for the inviscid problem is therefore obtained by solving some, as yet undetermined, viscous problem upstream and matching the two solutions. This could, in turn, lead to an inviscid solution quite different to that found by Kao (1970).

In the experiments of Debler (1959) the upstream boundary condition was not allowed to develop naturally but was forced to be of the form $\rho U_\infty^2 =$ constant. Hence, although the experiments were an excellent check on Kao's (1970) solution, they do not throw any light on whether the slip-line solution with $\rho U_\infty^2 =$ constant is the correct limiting solution close to the sink for a long withdrawal layer.

Koh (1966) investigated sink flow in a linearly stratified diffusive fluid of infinite extent. He neglected the inertia forces and made the usual boundary-layer-type simplifications. The flow was found to be self-similar and the solution exhibited a horizontally layered flow towards the sink. The thickness of the central layer, δ, was of order $(\nu D/\epsilon g)^{\frac{1}{4}}$, where ν is the coefficient of viscosity and D is the coefficient of salt or heat diffusion. The flow was forced to conserve volume flux through a vertical section, but, as is shown in the appendix to this paper, the momentum flux is not conserved. The reason why his results agree quite well with his experimental findings will become evident in the next section, where the overall structure of the layer is examined.

This paper considers the selective withdrawal from a very long reservoir with a depth sufficiently great for the induced velocities far from the sink to be small. The above known solutions are therefore in some sense either near-field or far-field solutions, but they do not match each other, nor does the far-field solution satisfy constancy of momentum flux. The following analysis examines the overall structure of such a layer with proper matching of the different regions in the limit of small Froude and Rayleigh numbers and large Reynolds number.

2. Structure of the withdrawal layer

The Boussinesq assumption is valid when $\epsilon L \ll 1$, where L is a typical vertical scale of the motion. It will become clear from later details of this analysis that inertia is only important close to the sink, where the thickness of the layer will be shown to be of order $q^{\frac{1}{2}}/(g\epsilon)^{\frac{1}{4}}$. Obviously, variations of the inertia force are only important when the mean inertia force is non-negligible, so that the Boussinesq approximation is valid provided that $q^{\frac{1}{2}}\epsilon^{\frac{3}{4}}/g^{\frac{1}{4}} \ll 1$. For typical reservoir operation this is of $O(10^{-4})$.

Consider the geometry shown in figure 1. The introduction of horizontal boundaries has two advantages. First, it yields a more realistic geometrical representation of a real reservoir. Second, it admits a solution, valid far from the sink, which conserves momentum flux. The type of walls which fulfill these requirements are ones which are stress free and along which ρ is constant. More complex boundary conditions could be treated in a similar way but boundary layers at a no-slip wall would further complicate the analysis.

Under the above assumptions the equations of motion become

$$\nabla . \mathbf{u} = 0, \tag{1}$$

$$\rho_0 \mathbf{u} . \nabla \mathbf{u} + \nabla p = -\rho g \hat{\mathbf{k}} + \mu \nabla^2 \mathbf{u}, \tag{2}$$

$$\mathbf{u} . \nabla \rho - \epsilon \rho_0 w = D \nabla^2 \rho. \tag{3}$$

The boundary conditions to be applied are

$$\boldsymbol{\tau}(x, \pm l) = 0, \quad \rho(x, \pm l) = 0, \tag{4), (5)}$$

$$u(\infty, z) = -q/2l, \quad w(x, \pm l) = 0, \quad u(0, z) = -q\delta(z), \tag{6), (7), (8)}$$

where D is the diffusion coefficient, $\boldsymbol{\tau}$ is the wall shear stress, u and w are the horizontal and vertical fluid velocities and $\delta(z)$ is the Dirac delta function. The density has been separated into $\rho_0 + \rho_e(z) + \rho(x, z)$, where ρ_0 is the mean density, $\rho_e(z)$ the ambient variation and $\rho(x, z)$ the motion-induced density change. The quantity ϵ is here defined by $-(1/\rho_0)\, d\rho_e/dz$ and p is the pressure minus the ambient equilibrium pressure. Finally, the Boussinesq assumption implies that the flow will be symmetric about the line $z = 0$.

2.1. *Outer flow*

It is assumed that the reservoir depth is sufficiently great so that at large distances from the sink the flow will be very slow and its development into a layered structure will not be influenced by inertia forces. In such cases the fluid will undergo three distinct flow transitions as it moves towards the sink. Very far upstream the imposed slip walls cause the flow to be uniform. This slow flow then becomes layered by the action of buoyancy. As this layer approaches the sink it becomes thinner, and at some critical distance from the sink inertia forces become comparable to the buoyancy forces. The subsequent flow in the layer will be governed by a balance of inertia, buoyancy and viscous forces.

The correct scaling of the vertical co-ordinate in the outer region, the inertia-free flow, would be a stretching by $R^{\frac{1}{3}}$, where R, equal to $(\nu D/\epsilon g l^4)^{\frac{1}{3}}$, is the Rayleigh number. However, this would also affect the wall spacing, which in turn would interfere with the far-field uniform flow. A more convenient scaling of the problem is obtained by shrinking the horizontal co-ordinate by an amount R. However, in doing this it must be remembered that for the purposes of matching with the inner flow the true outer co-ordinates are still $z/lR^{\frac{1}{3}}$ and x/l, and not z and Rx. Let

$$X = xR/l, \quad Z = z/l, \quad P = p/\rho_0 q(\epsilon g)^{\frac{1}{2}}, \quad \Lambda = \rho/F\epsilon\rho_0 l$$

and the scaled stream function $\Psi = \psi/q$, where l is the duct half depth. This scaling of the pressure and the density is dictated by the desire to have the pressure forces of the same magnitude as the buoyancy forces, and for the non-linear terms in the momentum equation (2) to be of the same order as those in the diffusion equation (3).

In terms of these new variables (1)–(3) become

$$F(\Psi_Z \Psi_{ZX} - \Psi_X \Psi_{ZZ}) + P_X = G\Psi_{ZZZ} + R^2 G \Psi_{ZXX}, \tag{9}$$

$$R^2 F(-\Psi_Z \Psi_{XX} + \Psi_X \Psi_{XZ}) + P_Z = -\Lambda - R^2 G \Psi_{XZZ} - R^3 G \Psi_{XXX}, \tag{10}$$

$$F(\Psi_Z \Lambda_X - \Psi_X \Lambda_Z) + \Psi_X = (1/G)\Lambda_{ZZ} + (1/G) R^2 \Lambda_{XX}, \tag{11}$$

where $F = q(g\epsilon)^{-\frac{1}{2}} l^{-2}$, $R = (\nu D/\epsilon g)^{\frac{1}{2}} l^{-2}$ and $G = (\nu/D)^{\frac{1}{2}}$.

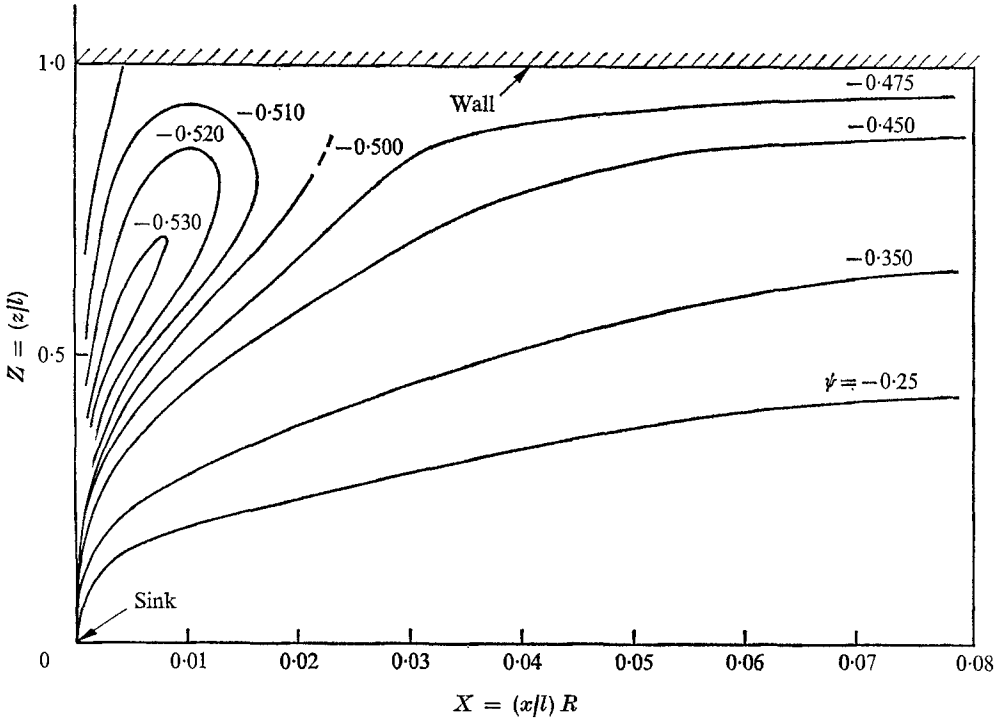

FIGURE 2. Outer solution.

The outer region equations are obtained by putting $R = 0$ and $F = 0$. These may then be combined to yield the equation for creeping flow obtained by Koh (1966):

$$\partial^6\Psi/\partial Z^6 + \partial^2\Psi/\partial X^2 = 0, \quad -1 \leqslant Z \leqslant 1, \quad 0 \leqslant X \leqslant \infty, \tag{12}$$

with the boundary conditions

$$\Psi(X, \pm 1) = \mp \tfrac{1}{2}, \tag{13}$$

$$\frac{\partial^2\Psi}{\partial Z^2}(X, \pm 1) = 0, \quad \frac{\partial^4\Psi}{\partial Z^4}(X, \pm 1) = 0 \tag{14), (15}$$

and

$$\Psi(0, Z) = -\tfrac{1}{2}\operatorname{sgn} Z. \tag{16}$$

Fourier analysis of (12) leads to the solution

$$\Psi(X, Z) = \frac{1}{\pi}\sum_{n=1}^{\infty} -\frac{1}{n} e^{-n^3\pi^3 X} \sin n\pi Z - \tfrac{1}{2}Z. \tag{17}$$

The streamlines are shown in figure 2. Convergence of the series is very rapid everywhere except at the origin, where it diverges.

To study the non-uniformity at the sink, it is necessary to know the limit of the above solution as $X \to 0$ and $Z \to 0$. This may be obtained conveniently by noting that

$$e^{-n^3\pi^3 X} = \int_{c-i\infty}^{c+i\infty} \frac{X^{-s}\Gamma(s)}{(\pi n)^{3s}}\, ds,$$

where c is a real constant greater than zero. Substituting for $e^{-n^3\pi^3X^3}$ in (17) and then expanding $\sin\pi Z$ in a power series yields the result

$$\Psi(X,Z) = -\frac{1}{\pi}\left\{\sum_{k=0}^{\infty}\frac{1}{3}\frac{(-1)^k}{(2k+1)!}\Gamma\left(\frac{2k+1}{3}\right)\zeta^{2k+1}\right\}+O(X)+O(Z^3), \tag{18}$$

where $\zeta = Z/X^{\frac{1}{3}}$.

In the appendix it is shown that the infinite series in (18) can be written in the form

$$\int_0^{\infty}\frac{1}{q}e^{-q^3}\sin q\zeta\, dq, \tag{19}$$

and that this is the solution found numerically by Koh (1966) for the unbounded fluid domain. Therefore, as the motion approaches the sink the outer flow changes from a uniform channel flow into Koh's (1966) self-similar motion.

2.2. *Inner flow*

The inner region occurs where the outer flow is sufficiently energetic for inertia to become important. It will be assumed that, just before this occurs, the flow will already have converged to a layer of thickness $O(R^{\frac{1}{3}})$ and that the outer variables are really $(x/l, z/lR^{\frac{1}{3}})$. Using these variables instead of X and Z leads to equations similar to (9)–(11) except that the nonlinear terms in (9) and (11) are multiplied by $F/R^{\frac{2}{3}}$ instead of F. One method of computing the horizontal extent of the inner region is to expand the stream function in a power series of $F/R^{\frac{2}{3}}$. An inspection of the second term of this series shows that the series diverges when x/l becomes smaller than

$$x_c = (F/R^{\frac{2}{3}})^{\frac{3}{2}}l,$$

or equivalently when X becomes smaller than $F^{\frac{3}{2}}$. In other words, for distances smaller than x_c the influence of inertia is not merely a correction to the outer flow, but it is the prime force. If $F/R^{\frac{2}{3}}$ is not small then the flow will become layered after inertia has become important. In contrast with the above, this would require keeping at least some representation of the inertia forces throughout the whole flow.

The correct inner variables are therefore

$$\xi = X/F^{\frac{3}{2}}, \quad \eta = Z/F^{\frac{1}{2}}. \tag{20), (21}$$

The outer solution $\Psi(x/l, z/lR^{\frac{1}{3}})$ when rewritten in terms of the inner variables is $\Psi((F/R^{\frac{2}{3}})^{\frac{3}{2}}\xi, (F/R^{\frac{2}{3}})^{\frac{1}{2}}\eta)$. Now as $F/R^{\frac{2}{3}}\to 0$, this becomes $\Psi(\zeta)$, where $\zeta = \eta/\xi^{\frac{1}{3}}$, hence the inner stream function remains unscaled, a condition required if all the flow is to pass through the layer. Because $\Lambda\to 1/X^{\frac{1}{3}}h(\zeta)$ as $X\to 0$ and $Z\to 0$, Λ must be scaled such that $\Pi = \Lambda F^{\frac{1}{2}}$. The equations in terms of these inner variables are

$$\Psi_\eta\Psi_{\eta\xi} - \Psi_\xi\Psi_{\eta\eta} + P_\xi = G\Psi_{\eta\eta\eta} + \frac{G}{R_e^2}\Psi_{\eta\xi\xi}, \tag{22}$$

$$\frac{1}{R_e^2}(-\Psi_\eta\Psi_{\xi\xi} + \Psi_\xi\Psi_{\xi\eta}) + P_\eta = -\Pi - \frac{G}{R_e^2}\Psi_{\xi\eta\eta} - \frac{G}{R_e^4}\Psi_{\xi\xi\xi}, \tag{23}$$

$$\Psi_\eta\Pi_\xi - \Psi_\xi\Pi_\eta + \Psi_\xi = \frac{1}{G}\Pi_{\eta\eta} + \frac{1}{GR_e^2}\Pi_{\xi\xi}, \tag{24}$$

where $R_e = q/\nu$.

In the limit $R_e \to \infty$, (22)–(24) reduce to

$$\Psi_\eta \Psi_{\eta\xi} - \Psi_\xi \Psi_{\eta\eta} + P_\xi = G\Psi_{\eta\eta\eta}, \tag{25}$$

$$P_\eta = -\Pi, \tag{26}$$

$$\Psi_\eta \Pi_\xi - \Psi_\xi \Pi_\eta - \Psi_\xi = (1/G)\,\Pi_{\eta\eta}, \tag{27}$$

which constitute the required inner equations for the limit $R \to 0$, $F \to 0$, $R_e \to \infty$ and $F/R^{\frac{3}{2}} \to 0$. Equations (25)–(27) must now be solved with the solution (18) as the upstream boundary condition.

It is interesting to note that (25)–(27) include the outer equations, and hence for those regions in which the wall influence is absent, the flow only depends on the parameter G. Any experimental flow at a given value of G is therefore self-similar with respect to the co-ordinates (ξ, η). The experiments described in § 4 verify this result very well (see figure 10).

The reason why R_e should be large for the above equations to be valid is perhaps best seen by examining the width-to-length ratio of the region of non-uniformity. The physical width δ of the region is of order $F^{\frac{1}{2}}l$ and the physical length x_c is of order $F^{\frac{3}{2}}l/R$. Hence

$$\frac{\delta}{x_c} = \frac{F^{\frac{1}{2}}R}{F^{\frac{3}{2}}} = \frac{R}{F} = \left(\frac{D}{\nu}\right)^{\frac{1}{2}} \cdot \frac{\nu}{q} = \frac{1}{G}\frac{1}{\sqrt{R_e}},$$

and thus $\delta/x_c \ll 1$ only if R_e is large. When R_e is small, (25)–(27) are nowhere valid and the flow near the sink is governed by the full Navier–Stokes equations.

In the next section equations (25)–(27) will be solved approximately by an integral method. For $\xi = \infty$, the withdrawal-layer thickness δ is matched to the inner limit of the outer solution. The boundary condition to be applied at $\xi = 0$ is obtained from an investigation of the flow near the sink. If the ξ variable is stretched by R/F (i.e. for outer variable distances closer than $O(F^{\frac{1}{2}})$) the equations of motion to first order in $1/R_e$ reduce to the Boussinesq approximation of the Euler equations for a stratified fluid. The solution of these equations would naturally depend on the solution of (25)–(27) and *vice versa*. Neither set admits a similarity solution, nor do they appear to be tractable by other methods. It was pointed out in the introduction that for the very special upstream condition of uniform flow Kao (1970) has solved the Euler equations. Here a slip line is required at the edge of the layer. The velocity along this slip line remains constant and of order $q^{\frac{1}{2}}(\epsilon g)^{\frac{1}{4}}$, which means that around this slip line there is a backward growing viscous–buoyancy layer of thickness $O(R^{\frac{1}{3}})$. However, at the moment it is a matter of speculation whether these two layers could be matched onto a solution of (25)–(27). The boundary condition of $\xi = 0$ is therefore somewhat uncertain, but the author believes that a realistic result may be obtained by using the condition, obtained by Kao (1970), that δ is equal to $F^{\frac{1}{2}}$ at $\xi = 0$. This is further justified in the discussion, and as long as the solution is not very sensitive to the exact numerical value of δ at $\xi = 0$, this procedure should lead to satisfactory results.

3. An integral solution estimate of δ

The equations to be solved are obtained by eliminating the pressure P from (25) and (27). In terms of the velocities U and W these are

$$(UU_\xi + WU_\eta)_\eta - \Pi_\xi - GU_{\eta\eta\eta} = 0, \tag{28}$$

$$U\Pi_\xi + W\Pi_\eta - W - (1/G)\,\Pi_{\eta\eta} = 0. \tag{29}$$

The boundary conditions are that Π, U, W and their appropriate derivatives tend to zero as $\eta \to \pm\infty$. The initial conditions are supplied at $\xi = \infty$ by the outer solution. For the purposes of the integral method it is more convenient to replace the boundary condition $W = 0$ as $\eta \to \pm\infty$ by the integral condition

$$\int_{-\infty}^{\infty} U\,d\eta = -1. \tag{30}$$

Examination of the experimental data obtained by Koh (1966) shows that, for a particular discharge, the velocity profiles are nearly self-similar even in the inner region. In § 4 this is confirmed in the more general co-ordinates (ξ, η). This suggests letting

$$U(\xi, \eta) = a(\xi) f(\eta/\delta(\xi)) \tag{31}$$

and obtaining f from the upstream flow. However, in that solution $\Pi = O(1/\eta)$ for large η, which is non-integrable. To be able to apply an integral method the equations must therefore be premultiplied by a weighting function. This is more easily done if f is an algebraic expression. It is therefore convenient to let

$$U(\xi, \eta) = \frac{-a(\xi)}{\pi} \frac{1 - k\eta^2\delta^{-2}}{(1+\eta^2\delta^{-2})^3}, \tag{32}$$

$$\Pi(\xi, \eta) = \frac{-b(\xi)}{\pi} \frac{\eta\delta^{-1}}{1+\eta^2\delta^{-2}}, \tag{33}$$

where k is a constant. By conservation of mass

$$W = \frac{-\delta'\eta a}{\pi\delta} \frac{(1-k)\,\eta^2\delta^{-2}}{(1+\eta^2\delta^{-2})^3}. \tag{34}$$

The value of the constant k is then chosen to yield the best fit to the similarity solution (18). The unknown functions are $a(\xi)$, $b(\xi)$ and $\delta(\xi)$.

Equations (32)–(34) are now substituted into the following integral form of (28)–(29):

$$\int_{-\infty}^{\infty} \frac{1}{(1+\eta^2\delta^{-2})} \{(UU_\xi + WU_\eta)_\eta - \Pi_\xi - GU_{\eta\eta\eta}\}\,d\eta = 0, \tag{35}$$

$$\int_{-\infty}^{\infty} \left\{U\Pi_\xi + W\Pi_\eta - W - \frac{1}{G}\,\Pi_{\eta\eta}\right\} d\eta = 0, \tag{36}$$

$$\int_{-\infty}^{\infty} U\,d\eta = -1. \tag{37}$$

The factor $1/(1+\eta^2\delta^{-2})$ is included in (35) to make Π_ξ integrable. Carrying out the integration yields two ordinary differential equations and one algebraic

equation for a, b and δ. The variables a and b may be eliminated from these equations, resulting in a single equation for δ:

$$(\alpha_1\delta^5-\alpha_2\delta)\,\delta''+(\alpha_1\delta^4+3\alpha_2)\,\delta'^2+\alpha_3\delta'+\alpha_4=0, \tag{38}$$

where
$$\alpha_1=\frac{1-k}{3-k},$$

$$\alpha_2=\frac{128}{3}\frac{1}{\pi^2}\frac{2-k}{(3-k)^2}\left(\frac{6}{7}+\frac{k}{21}-\frac{k^2}{105}\right),$$

$$\alpha_3=\frac{64}{\pi}\frac{1}{(3-k)^2}\left(\frac{6}{7}+\frac{k}{21}-\frac{k^2}{105}\right)\frac{1}{G}+\frac{16}{5\pi}\frac{2-k}{(3-k)^2}(11k+32)\,G$$

and
$$\alpha_4=\frac{8}{5}\frac{11k+32}{3-k}.$$

The boundary conditions are that $\delta=1$ at $\xi=0$ and that, as $\xi\to\infty$, δ approaches the value of the solution of (38) with the inertia terms set to zero. The differential equation for δ, obtained by ignoring the inertia terms in (38), is

$$\alpha_1\delta^5\delta''+\alpha_1\delta^4\delta'^2+\alpha_4=0. \tag{39}$$

Letting $p=\delta^2$ gives
$$p^2\frac{d^2p}{d\xi^2}+\frac{2\alpha_4}{\alpha_1}=0, \tag{40}$$

which is the Emden–Fowler equation. Bellman (1953) has shown that all solutions to this equation are asymptotic to the solution

$$p=K_1^2\xi^{\frac{2}{3}}, \tag{41}$$

where $K_1(9\alpha_4/\alpha_1)^{\frac{1}{3}}$, so that
$$\delta\sim K_1\xi^{\frac{1}{3}}, \tag{42}$$

as required. To reduce the numerical integration, further terms of the asymptotic series were found, namely,

$$\delta=K_1\xi^{\frac{1}{3}}+K_2\xi^{-\frac{1}{3}}+K_3\xi^{-\frac{2}{3}}+K_4\xi^{-1}+K_5\xi^{-\frac{4}{3}}+\ldots, \tag{43}$$

where
$$K_1=(9\alpha_4/\alpha_1)^{\frac{1}{3}},\quad K_2=3\alpha_3/4\alpha_1K_1^4,\quad K_3=\text{arbitrary},$$

$$K_4=(2/3\alpha_1K_1^5)\{\tfrac{1}{9}\alpha_1K_1^4K_2^2+\tfrac{1}{3}K_2\alpha_3-\tfrac{5}{9}K_1^2\alpha_2\}$$

and
$$K_5=(1/14K_1^5K_2)\{6K_3\alpha_3-22\alpha_1K_1^4K_2K_3\}.$$

The similarity of the series (43) to that proposed by Koh (1966) should be noted. However, the above contains extra terms which are all dependent on the arbitrary constant K_3. This free parameter is necessary as nothing has been said about the behaviour of the solution at $\xi=0$. Similarly, Koh's (1966) proposed series should have an equivalent arbitrary coefficient.

The arbitrary constant K_3 was used to convert the boundary-value problem into an initial-value problem. In other words, K_3 was fixed, δ and δ' were computed from the series (43) for a sufficiently large value of ξ and (38) was integrated numerically to the origin. The constant K_3 was adjusted until $\delta=1$ at $\xi=0$.

Inspection of (38) shows that it has a singular point when

$$\delta=\delta_c=(\alpha_2/\alpha_1)^{\frac{1}{4}}. \tag{44}$$

The slope of δ becomes infinite here and the assumption of a similar profile can no longer adequately describe the flow. The value of k was therefore chosen to

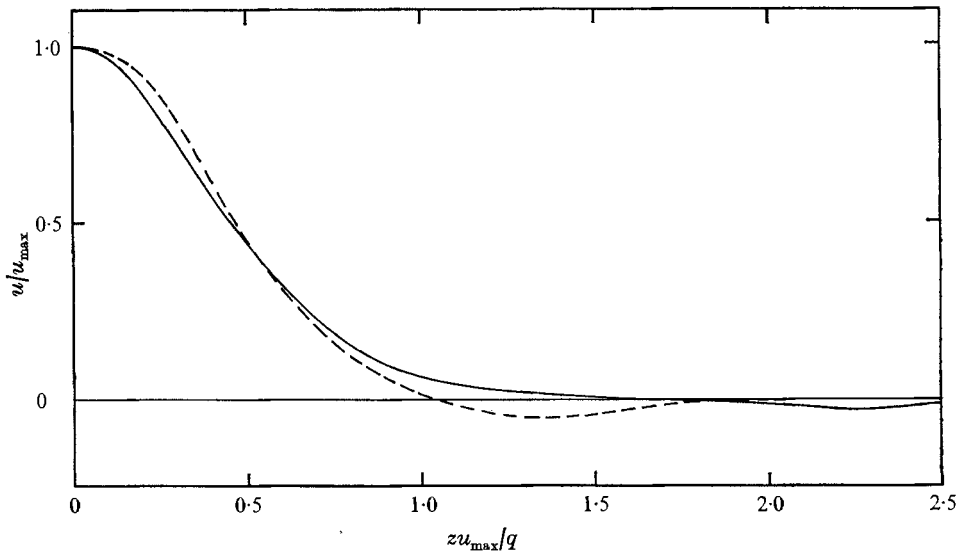

FIGURE 3. Comparison of the integral velocity profile with the velocity profile obtained by Koh (1966). ——, assumed integral profile; – – –, Koh (1966).

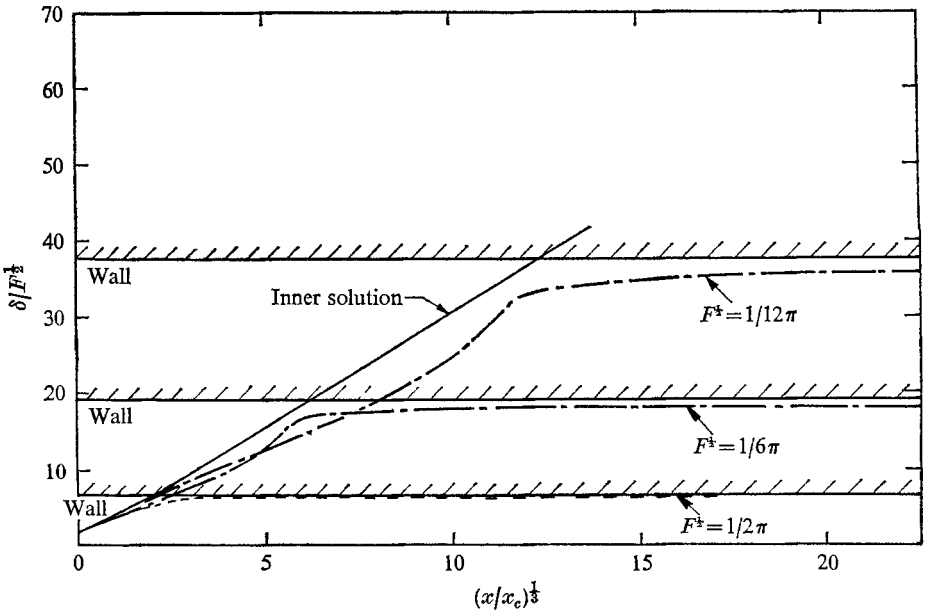

FIGURE 4. Composite solution for heat stratification with $G = 2{\cdot}34$. The position of the upper wall is a function of the Froude number because the inner vertical scale is $Z/F^{\frac{1}{2}}$. The x co-ordinate is non-dimensionalized with respect to the length of the inner region $x_c = (F^{\frac{3}{2}}/R)l$.

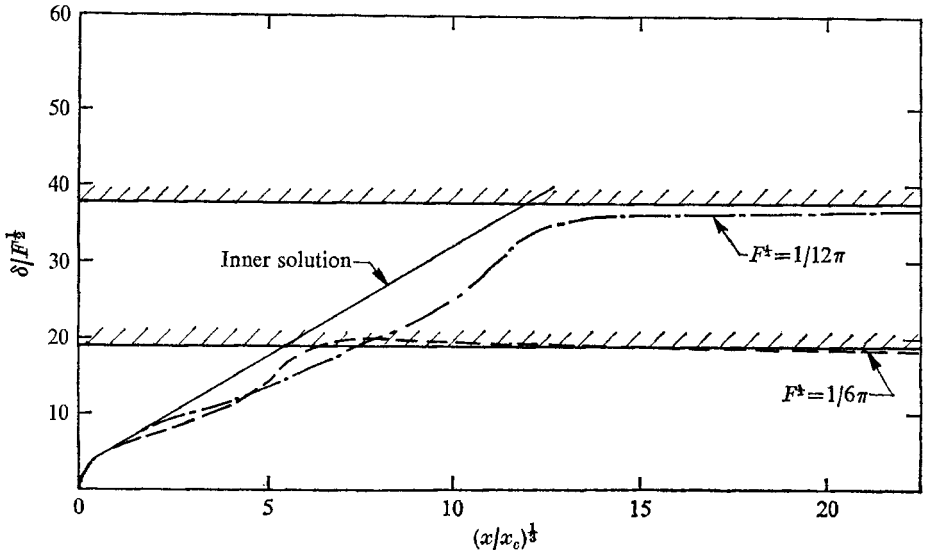

FIGURE 5. Composite solution for salt stratification with $G = 29{\cdot}0$. The position of the upper wall is a function of the Froude number because the inner vertical scale is $Z/F^{\frac{1}{2}}$. The x co-ordinate is non-dimensionalized with respect to the length of the inner region $x_c = (F^{\frac{2}{3}}/R)\,l$. Notice that the theory fails for values of $F^{\frac{1}{2}} > 1/6\pi$ as inertia is then no longer negligibly small far upstream.

make $\delta_c = 1$ and $K_1 = 3{\cdot}2$, the value obtained from (18) for the present definition of δ. The actual value adopted for k was $\frac{1}{3}$, which yielded values K_1 and δ_c of $3{\cdot}15$ and $1{\cdot}17$ respectively. Figure 3 shows a comparison of the velocity profile given by the integral curve (32) with that from equation (18).

The composite expansion δ was obtained by adding the inner and outer solution and subtracting $K_1\xi^{\frac{1}{3}}$, the part which is common to both. This is shown in figures 4 and 5 for both heat and salt stratification. Unfortunately the wall spacing in the outer problem does not scale with $F^{\frac{1}{2}}$, so that the wall 'moves' with respect to an inner (ξ, η) co-ordinate system as F changes. However, the advantage of this co-ordinate system is that near the sink the solution depends on G only. It should be noted that this sole dependence of the flow on G will extend to flows for which G is larger than unity. The reason for this is that (25)–(27) contain a representation of the total process and therefore contain the equation representing flow with negligible species diffusion as a subset.

Implicit throughout the above development is the fact that any inertia forces present become negligibly small far enough upstream. At large Froude numbers this limitation is violated and the composite layer may become thicker than the channel depth. For the case $F^{\frac{1}{2}} = 1/6\pi$ this is illustrated in figure 5.

4. Experimental verification

The experimental results obtained by Koh (1966) are shown replotted in figure 6. The withdrawal-layer thickness has been reduced by $0{\cdot}9$ from that used by Koh (1966) in order to correspond to the definition used in this paper. It is

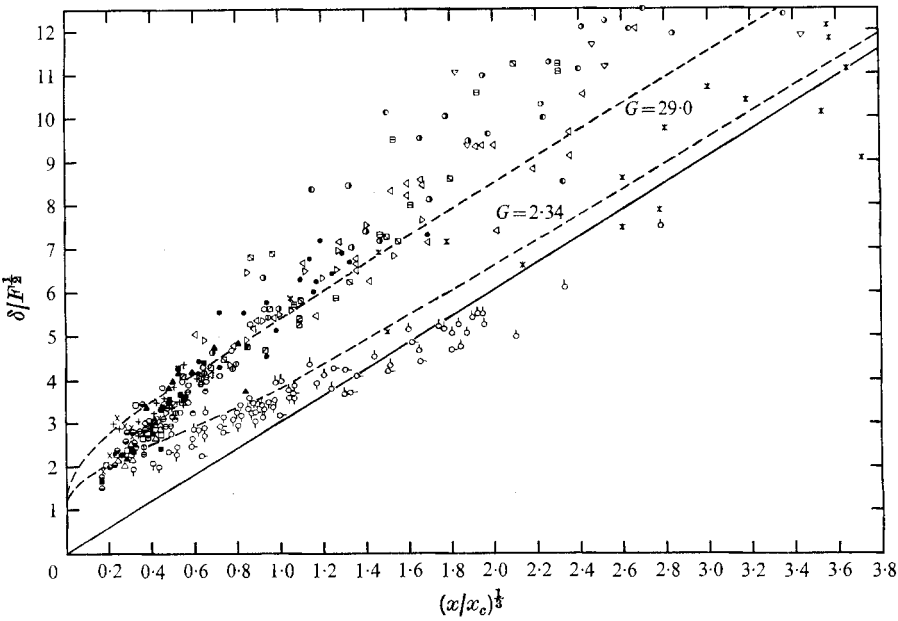

FIGURE 6. Withdrawal-layer thickness data after Koh (1966). The parameter G = 2·34 for heat-stratified water and G = 29·0 for salt-stratified water. ---, integral solution; ——, non-inertial integral solution.

Expt.	N-8-1·7	N-8-3·5	N-8-11·7	N-12-0·15	N-12-0·3	N-12-0·9
Expt.	N-12-2·3	N-12-4·4	N-12-10	N-25-0·04	N-25-0·2	N-25-0·5
Expt.	N-25-5	N-25-9	N-50-0·13	N-50-0·5	N-50-1	N-50-3
Expt.	N-50-6	N-50-11·6	T-16-0·6	T-18-20	T-21-2·4	T-10-5

seen that the two cases, salt and heat stratification, fall into two separate regions on the graph. The relatively large scatter can probably be attributed to the rather small depth and short length of Koh's (1966) experimental apparatus. It must be remembered that the theory was derived for the case when x_c is small compared with both the depth and length. In view of this, an experimental programme designed to repeat and extend Koh's data was carried out in a facility much larger than that used by Koh (1966). All the experiments were conducted in a salt stratified solution to avoid the side-wall-induced convection boundary layers present in a thermally stratified tank. A perfectly still reservoir was essential since the velocities in the withdrawal layers are extremely small.

4.1. *Apparatus and techniques*

The experimental procedure was in principle very similar to that used by Koh (1966) and only a brief description will be given. The experiments were performed

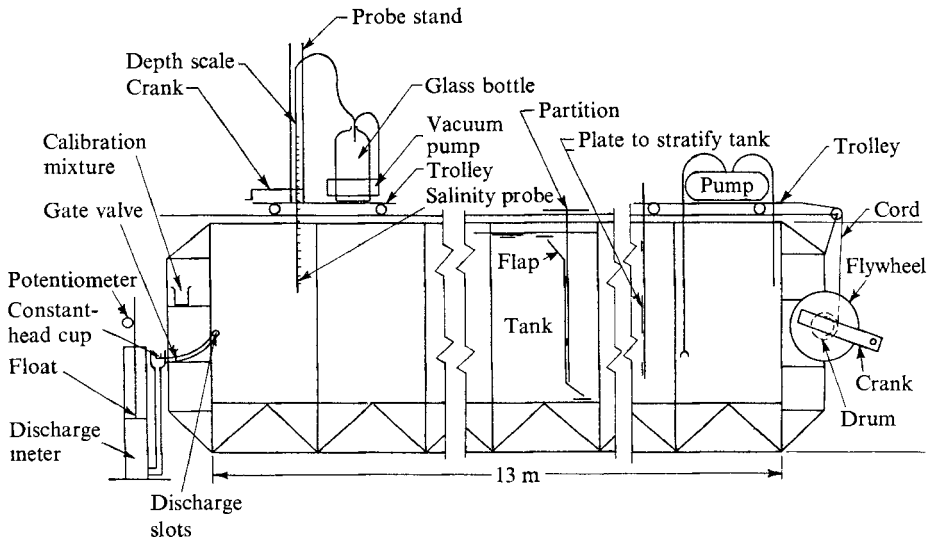

FIGURE 7. General layout of experimental tank.

in a 13 m long, 1 m deep, 45 cm wide tempered plate-glass tank. The tank is shown schematically in figure 7. Two trolleys were placed on rails on top of the tank; one served as a mounting platform for the stratifier while the other held the salinity probe and associated vacuum pump. The discharge facility was located at one end. Mounting the salinity probe on the trolley allowed the same probe to be used to measure the density gradients throughout the channel and the salinity of the discharging water.

The water was stratified by dissolving it in ordinary kiln-dried commercial salt. This proved to be pure enough as only the background density was measured; no attempt was made to measure the small fluctuations of salinity induced by the motion. The salinity was measured with a conductance probe connected to a paper chart recorder. The probe was calibrated with a set of reference solutions at the same temperature as the tank water.

The linear density profile was established by a slight modification of the method described by Clark *et al.* (1967). The whole tank was filled with fresh water and a gated partition was introduced vertically into the centre of the tank, preventing any transfer of water from one side to the other. The appropriate amount of salt was then stirred into one half of the partitioned tank and the water was mixed by pumping from the bottom to the top. Once the mixture was uniform it was allowed to come to rest. The flaps of the partition were then opened very slightly to allow the salt water to flow beneath the fresh water and the fresh water to flow over the salt water. About half an hour elapsed before the whole tank had a two-layer stratification in it. The partition was then carefully removed.

To obtain a linear profile, a series of three plates, mounted on the trolley, were then briskly moved through the interface with a crank and pulley arrangement at the end of the tank. The largest plate moved directly through the interface while the two smaller ones stirred up the top and bottom layers. The wakes behind

the plates created sufficient turbulence to allow mixing. The mixing smoothed out the interface, and after some adjustment of the position of the plates a very linear profile was obtained throughout the whole depth.

To ensure constant monitoring of the discharge flowing out through the sink a float type discharge meter was installed. This provided a means of adjusting the flow rate to a desired value and also of checking its constancy as the experiment proceeded. However, the actual discharge used in the reduction of the data was obtained by integrating the velocity profiles.

The velocities induced by the fluid withdrawal are of the order of a few centimetres per minute. For such low velocities a suitable method of velocity measurement was to drop crystals of dye into the centre of the tank at incremented distances from the sink. The purple streaks left in the wake of the falling crystals were then photographed repeatedly.

Of the dyes available, it was found that potassium permanganate was the most suitable for the present experiment. In contrast to organic dyes, this has the great advantage that it forms very fine intense streaks, the lifetime of which are only about a quarter of an hour. Their rapid decay, which is due to oxidation, allows experiments to be repeated quite quickly. The crystals used were about $\frac{1}{4}$–$\frac{1}{2}$ mm in diameter and care was taken to choose only the most spherical ones. The crystals were placed, after cutting, into a small recess in a wooden dowling at a spacing of about 10 cm. This wooden bar was then placed on top of the tank. To introduce the crystals into the water the bar was inverted.

The motion of the dye streaks was recorded photographically, the time between photographs being measured by simultaneously tripping the camera shutter and the event marker on the recorder. The negative images were enlarged to half scale on a plastic-base photographic paper allowing distances to be scaled off directly.

4.2. *Experimental results*

The no-slip condition on the side walls forced the layer to have a parabolic velocity variation across the width of the tank, rather than a uniform distribution as assumed in the theory. For this reason, the local discharge q_m, obtained by integrating the velocity profile with a planimeter, was used in the reduction of the data. To obtain q_m, successive photographs were aligned and the top profile was pricked through with a needle onto the other photograph. The area between the two curves of six roughly equally spaced profiles was then measured with a planimeter. The total net area was used rather than just the forward flowing part. To within 10 % the areas were the same and the mean of the six areas was used to calculate the discharge.

For the integral velocity profile, the velocity at $\eta = \delta$ is $\frac{1}{12}$ the centre-line velocity. This provides a convenient definition for δ in the experimental data as that width at which the velocity has dropped to $\frac{1}{12}$ the centre-line value. This value of δ was also much better defined on the photographs than the point where the velocity is zero. The profile has a large non-zero slope here, and it formed a definite intersection with the line $u = \frac{1}{12}u_{\max}$. The values of δ, measured as described, and the above value of q_m were then used to plot, as shown on figure 8,

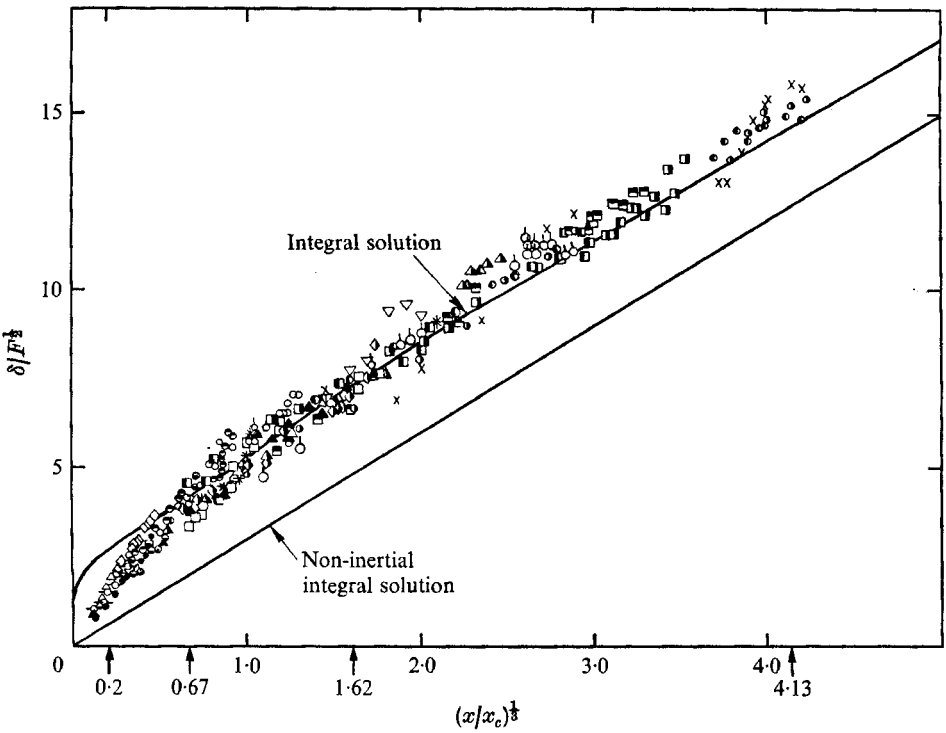

FIGURE 8. Experimental withdrawal-layer thickness for salt stratification with $G = 29{\cdot}0$. The parameter $x_c = (F^{\frac{2}{3}}/R)l$.

Expt.	1-1	1-2	1-3	2-1	2-2	2-3	3-1	3-2	3-3	3-4
Expt.	3-5	3-6	4-1	4-2	4-3	4-5	4-6	4-7	4-8	4-9

$\delta/F_m^{\frac{1}{2}}$ *vs.* $(x/x_c)^{\frac{1}{3}}$, where $x_c = (q/\nu)^{\frac{3}{2}}(\nu D/\epsilon g)^{\frac{1}{4}}$ and $F_m = q_m/(\epsilon g)^{\frac{1}{2}}$. The normalized velocity profiles at four values of (x/x_c) are shown in figure 9. The solid line again corresponds to the integral velocity distribution, which may be rewritten to have $u/u_{\max}$ as the ordinate and $zu_{\max}/q_m$ as the abscissa:

$$\frac{u}{u_{\max}} = \frac{1-0{\cdot}367(zu_{\max}/q_m)^2}{[1+1{\cdot}1(zu_{\max}/q_m)^2]^3}. \tag{45}$$

Figures 8 and 9 show little scatter, indicating that random errors due to parallax, enlarging and aligning of photographs are quite small. Furthermore, as long as the scale in the vertical direction, 2δ, is smaller than the width, and provided the local centre-line discharge q_m is used, the error introduced owing to three-dimensionality will be small. In the present experiments the ratio of thickness to width of the layer was kept to less than 0·1 by taking data only in the first 2 m of the tank. Data from four different values of the density gradient and about five different discharges for each value of ϵ are represented on figures 8 and 9.

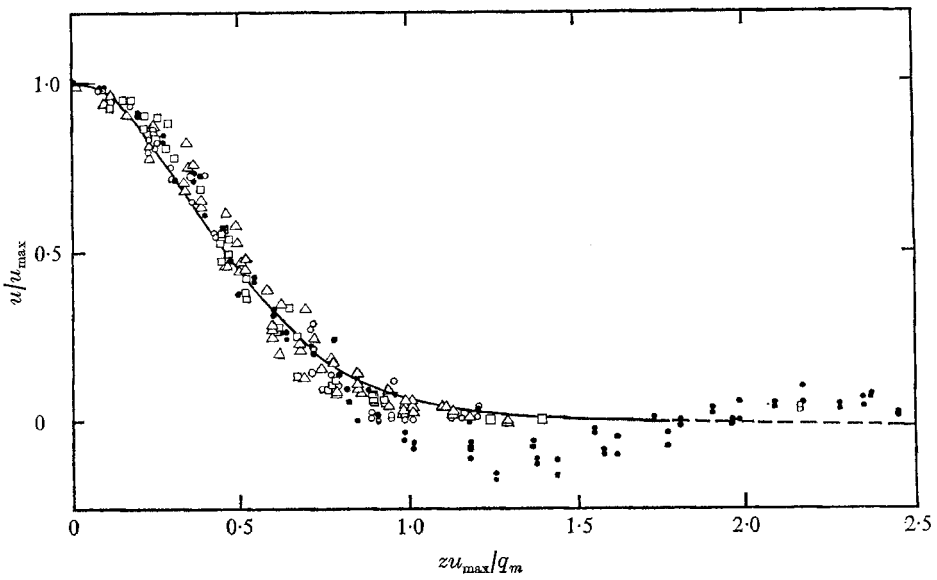

FIGURE 9. Experimental velocity profiles for salt stratification with $G = 29{\cdot}0$. —, integral profile; ●, $(x/x_c)^{\frac{1}{3}} = 4{\cdot}13$; ○, $(x/x_c)^{\frac{1}{3}} = 1{\cdot}62$; △, $(x/x_c)^{\frac{1}{3}} = 0{\cdot}67$; □, $(x/x_c)^{\frac{1}{3}} = 0{\cdot}20$.

The value of x_c was varied from 2 cm to 2 m but for most of the data x_c was less than 1 m. This ensured that the experiment adhered to the assumptions of the theory. The experimental programme is summarized in table 1.

5. Discussion

Theory showed that the flow should be independent of any parameter except G, when the x and z co-ordinates are scaled correctly. This is verified in figure 8, where the data are seen all to fall onto one curve for a particular G. The above observation is equally true for the salt stratification, where G is quite large, even though the theory was developed for G of order one. For the same reason a large value of G does not invalidate the integral-solution results. A comparison between the theory and experiment is shown in figure 8 and it can be considered good everywhere except near the sink. The difficulty here results from the still unknown behaviour of the flow very near the sink. There is a temptation to adjust K_3, the floating upstream constant, to improve the fit near the origin. Figure 10 shows curves for different values of K_3 and it is seen that the integral curve for $K_3 = -82{\cdot}2$ fits the data better than the originally adopted curve, which has $K_3 = -81{\cdot}8$. This is an encouraging flexibility of the method, but the original choice of K_3 remains the only theoretically justifiable one until a more definite solution for the flow very close to the sink is obtained to which the integral solution may be matched.

It was hoped that the velocity profile measurements would indicate some of the structure changes very close to the sink and clarify the nature of the inviscid core. Figure 9 shows, however, that even for x of the order of $F_m^{\frac{1}{2}}$ the velocity

Expt.	T_w (°C)	ν (10^{-5} cm^2 s^{-1})	D (10^{-5} cm^2 s^{-1})	ϵ (10^{-5} cm^{-1})	q (cm^2 s^{-1})	q_m (cm^2 s^{-1})	G approx.	F_m (cm^2)	$(\epsilon g/\nu D)^{\frac{1}{2}}$ (10^3 cm^{-2})	x_c (cm)
1-1	14	1120	1·25	2·98	0·210	0·225	29	1·31	0·458	688
1-2	14	1120	1·25	2·98	0·320	0·366	29	2·14	0·458	1439
1-3	14	1120	1·25	2·98	0·454	0·496	29	2·90	0·458	2260
2-1	20	1000	1·25	25·7	0·006	0·012	29	0·024	1·46	5·4
2-2	20	1000	1·25	25·7	?	0·062	29	0·124	1·46	64·3
2-3	20	1000	1·25	25·7	?	0·272	29	0·543	1·46	584·0
3-1	14	1120	1·25	29·9	0·005	0·007	29	0·013	1·45	2·18
3-2	15	1100	1·25	29·9	0·013	0·014	29	0·026	1·46	6·43
3-3	15	1100	1·25	29·9	0·031	0·033	29	0·062	1·46	22·8
3-4	18	1040	1·25	29·9	0·064	0·073	29	0·136	1·50	25·0
3-5	18	1040	1·25	29·9	0·118	0·143	29	0·264	1·50	204·0
3-6	18	1040	1·25	29·9	0·185	0·233	29	0·429	1·50	420·0
4-1	14	1120	1·25	35·3	0·006	0·007	29	0·012	1·57	2·14
4-2	14	1120	1·25	35·3	0·005	0·007	29	0·012	1·57	2·22
4-3	16	1080	1·25	35·3	0·007	0·010	29	0·017	1·60	3·81
4-5	16	1080	1·25	35·3	0·009	0·011	29	0·019	1·60	4·38
4-6	16	1080	1·25	35·3	0·012	0·013	29	0·022	1·60	5·85
4-7	14	1120	1·25	35·3	0·017	0·020	29	0·034	1·57	9·90
4-8	14	1120	1·75	35·3	0·022	0·024	29	0·041	1·57	13·40
4-9	14	1120	1·25	35·3	0·037	0·044	29	0·075	1·57	32·2

TABLE 1. Summary of basic experimental parameters

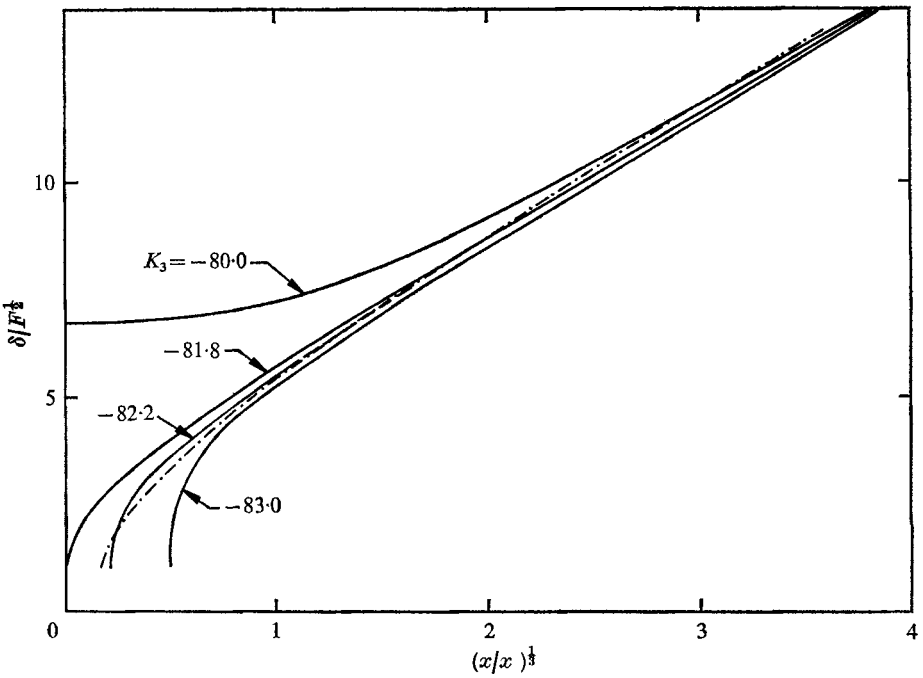

FIGURE 10. Variation of the integral solution with the constant K_3. —·—, experimental value (line of best fit).

profiles are self-similar to those for large x/x_c. The only change is that the back-flow velocity decreases, in relation to the centre-line velocity, as x is decreased or, equivalently, as q is increased. Further work, both experimental and theoretical, is needed to describe the flow close to the sink.

The rate of mass leaving the duct at the sink is, by symmetry, equal to $(\rho_e(0)+\rho_0)q$, which in turn is equal to mass flow rate at infinity

$$\int_{-l}^{l} u_\infty(\rho_0+\rho_e)\,dz.$$

In other words, the withdrawal is not really selective at all, but rather is the result of a diffusion averaging process extending over the whole flow region.

Tests conducted by the Tennessee Valley Authority on some of their reservoirs appear to be the only source of actual reservoir data. The work summarized in the T.V.A. reports (1969*a* *Water Resources Res. Lab. Rep.* no. 4, 1–8; 1969*b* *Water Resources Res. Lab. Rep.* no. 13, 1–30) is concerned with the measurement of the velocity, temperature and water oxygen content distribution in a reservoir from which water is being drained. These results are shown in figure 11.

The difficulty of measuring velocities is caused by the unsteady nature of the operating discharge and the irregular geometry of most reservoirs. Furthermore, the reservoir discharges were always very high and when combined with the molecular values of ν and D yielded values of x_c ten to one hundred times larger than the length of the reservoirs. This means that the inertial region extends over

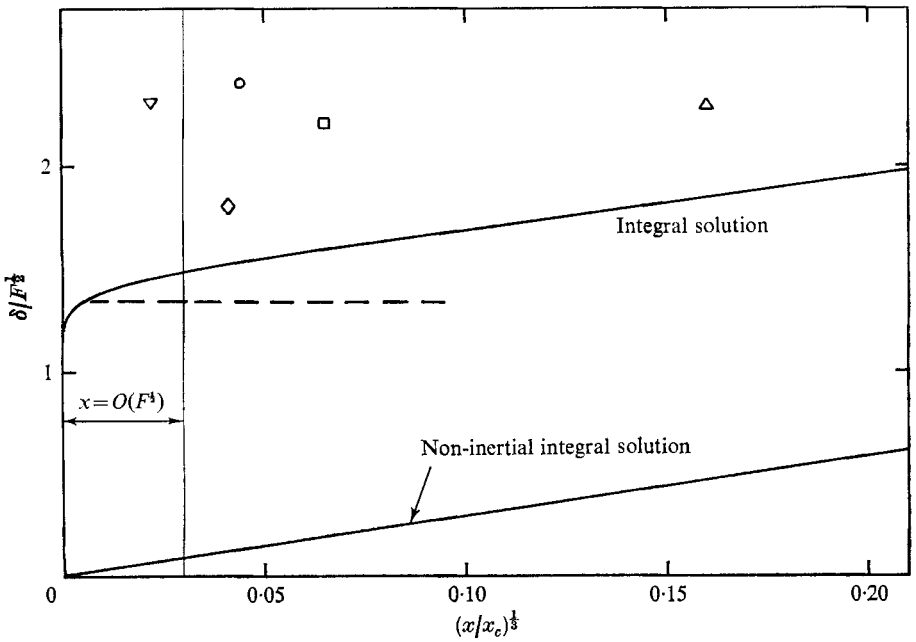

FIGURE 11. Prototype experimental data from T.V.A. Water Resources Research Reports. ———, layer thickness in an inviscid fluid; ▽, Fontana; ◇, ○, □, △, Cherokee.

the whole reservoir. Consequently the outer solution is valid nowhere in the reservoir. Brooks & Koh (1969), in an effort to explain the difference between the observed withdrawal-layer thickness and that predicted by Koh (1966), postulated eddy transport coefficients much larger than their molecular counterparts. The use of Koh's (1966) solution is now seen to be incorrect, but a similar procedure can be used for the present theory. An increase in ν and D decreases x_c and this moves the data points to the right in figure 11. With the assumption that $\nu = D$, a typical value of the eddy transport coefficient sufficient to move the data onto the theoretial curve is $10^{-1}\,\mathrm{cm^2\,s^{-1}}$. This is an increase by a factor of 10^2 over the molecular values leading to transport coefficients compatible with the measurements of Orlob & Selna (1970). The value of x_c, based on such transport coefficients, corresponds roughly to the length of the reservoir but is still much larger than the depth.

The weakness of the above procedure is that, as yet, there is no explanation of a mechanism which could sustain these larger eddy transport coefficients. Measurements (T.V.A. 1969*b*) of the local Richardson number with depth, for a typical run, indicate that this varies between 10 and 10 000, values which are much too high for local shear instability.

The large values of x_c encountered in reservoirs with peak discharges also means that the end walls cannot be neglected and these could have first-order effects on the thickness of the layer; an end wall stops the withdrawal layer and much larger reverse flows are induced. A large discharge could thus cause a vigorous layer to extend to the rear wall and this would induce a reverse layer above and below

the centre layer. Schiff (1966), in a related problem, has found that this induced snaking of the flow with possible mixing at the boundaries leads to increased diffusion of the species. In the present problem this would increase G and thus increase the thickness of the layer.

In summary it can be said that the theory, although yielding good agreement with laboratory experiments, is still not able to explain completely prototype behaviour. However, it does yield a rational basis from which to proceed to include the effects of larger eddy transport coefficients and end-wall effects.

This work is part of a Ph.D. thesis submitted to the University of California, Berkeley. The author would like to thank his advisor, Prof. H. B. Fischer, for his assistance and encouragement throughout and Prof. G. Corcos for the many hours of discussion extended to him. This work was undertaken while the author was a recipient for two years of a Gledden Fellowship award from the University of Western Australia. In the third year the author held a Science Fellowship from the University of California. The experimental programme was supported by a grant from the Environmental Protection Agency under Contract no. 15040 EJZ.

Appendix

The linearized equations governing the motion far from the sink were shown to be

$$P_X = \Psi_{ZZZ}, \quad P_Z = -\Lambda, \quad \Psi_X = \Lambda_{ZZ}, \qquad \text{(A 1), (A 2), (A 3)}$$

where Ψ, P and Λ are the scaled stream function, pressure and density, respectively. For convenience the parameter G has been set equal to one. The solution of this set of equations is now given for a domain extending in both the vertical and horizontal directions to infinity.

Let

$$\Psi = f(\zeta), \quad P = P(\zeta), \quad \Lambda = (1/X^{\frac{1}{3}})\,h(\zeta), \qquad \text{(A 4), (A 5), (A 6)}$$

where $\zeta = Z/X^{\frac{1}{3}}$. After eliminating the pressure, (A 1)–(A 3) become

$$g'' = \tfrac{1}{3}\zeta h + g''(0) \qquad \text{(A 7)}$$

and

$$h'' = -\tfrac{1}{3}\zeta g, \qquad \text{(A 8)}$$

where $g = f'$. The boundary conditions to be applied are

$$\int_{-\infty}^{\infty} g(\zeta)\,d\zeta = -1,$$

$$h, g, g' \to 0 \quad \text{as} \quad \zeta \to \pm\infty$$

and that g is an even function of ζ.

Eliminating h from (A 7) and (A 8) leads to the following fifth-order equation for g:

$$g^{\mathrm{v}} + \tfrac{1}{9}\zeta^2 g' + \tfrac{4}{9}\zeta g = 0. \qquad \text{(A 9)}$$

A solution of (A 9) satisfying the above boundary conditions is given by

$$g(\zeta) = \frac{1}{\pi}\int_0^{\infty} e^{-q^3}\cos q\zeta\,dq, \qquad \text{(A 10)}$$

or alternatively

$$f(\zeta) = \frac{1}{\pi}\int_0^\infty \frac{1}{q} e^{-q^3} \sin q\zeta \, dq. \tag{A 11}$$

A power-series representation of f is given by expanding the sine term and integrating term by term and yields

$$f(\eta) = -\frac{1}{\pi}\left\{\sum_{k=0}^{\infty} \frac{(-1)^k}{(2k+1)!}\frac{1}{3}\frac{\Gamma(2k+1)}{3}\eta^{2k+1}\right\}. \tag{A 12}$$

It should be noted that the integral form of the x momentum equation must hold as well as the condition $\Psi(\infty) - \Psi(-\infty) = 1$. In the present model the former simplifies to

$$\int_{-\infty}^{\infty} P\,dZ = J. \tag{A 13}$$

where J is a constant. Substituting for the pressure yields

$$J = +X^{\frac{1}{3}}\int_{-\infty}^{\infty} P(\zeta)\,d\zeta. \tag{A 14}$$

Hence not only does J become unbounded, but also $\partial J/\partial X$ is not zero, and this type of pressure variation violates the integral statement of the simplified momentum equation.

REFERENCES

Bellman, R. 1953 *Stability Theory of Differential Equations.* McGraw-Hill.

Brooks, N. H. & Koh, R. C. Y. 1969 *J. Hyd. Div. Proc. A.S.C.E.* **95** (HY4), 1369–1400.

Clark, C. B., Stockhausen, P. J. & Kennedy, J. F. 1967 *J. Geophys. Res.* **72,** 1393–1395.

Debler, W. R. 1959 *J. Eng. Mech. Div. Proc. A.S.C.E.* **85,** 673–695.

Kao, T. W. 1965 *J. Fluid Mech.* **21,** 535–543.

Kao, T. W. 1970 *Phys. Fluids,* **13,** 558–564.

Koh, R. C. Y. 1966 *J. Fluid Mech.* **24,** 555–575.

Orlob, G. T. & Selna, L. G. 1970 *J. Hyd. Div. Proc. A.S.C.E.* **96** (HY2), 391–410.

Schiff, L. L. 1966 *Deep Sea Res.* **13,** 621–626.

Yih, C.-S. 1965 *Dynamics of Nonhomogeneous Fluids.* Macmillan.